The EMBO Journal (2007) 26, 527–537 | © 2007 European Molecular Biology Organization | All Rights Reserved 0261-4189/07
www.embojournal.org

THE EMBO JOURNAL

Counting of six pRNAs of phi29 DNA-packaging motor with customized single-molecule dual-view system

Dan Shu[1,3], Hui Zhang[1,3], Jiashun Jin[2] and Peixuan Guo[1,*]

[1]Department of Comparative Pathobiology and Weldon School of Biomedical Engineering, Purdue University, West Lafayette, IN, USA and [2]Department of Statistics, Purdue University, West Lafayette, IN, USA

Direct imaging or counting of RNA molecules has been difficult owing to its relatively low electron density for EM and insufficient resolution in AFM. Bacteriophage phi29 DNA-packaging motor is geared by a packaging RNA (pRNA) ring. Currently, whether the ring is a pentagon or hexagon is under fervent debate. We report here the assembly of a highly sensitive imaging system for direct counting of the copy number of pRNA within this 20-nm motor. Single fluorophore imaging clearly identified the quantized photobleaching steps from pRNA labeled with a single fluorophore and concluded its stoichiometry within the motor. Almost all of the motors contained six copies of pRNA before and during DNA translocation, identified by dual-color detection of the stalled intermediates of motors containing Cy3-pRNA and Cy5-DNA. The stalled motors were restarted to observe the motion of DNA packaging in real time. Heat-denaturation analysis confirmed that the stoichiometry of pRNA is the common multiple of 2 and 3. EM imaging of procapsid/pRNA complexes clearly revealed six ferritin particles that were conjugated to each pRNA ring.

The EMBO Journal (2007) **26,** 527–537.
doi:10.1038/sj.emboj.7601506
Subject Categories: microbiology & pathogens
Keywords: biomotor; bionanotechnology; nanobiotechnology; SMDV-TIRF; RNA nanotechnology

Introduction

One striking feature in the assembly of linear dsDNA viruses is that their lengthy genome is translocated into the limited space within the preformed protein coat and packaged to near-crystalline density (Guo, 1994; Lin and Black, 1998; Cue and Feiss, 2001). This entropically unfavorable DNA translocation task is accomplished by an ATP-driven motor involving two nonstructural components with specific characteristics typical of ATPases (Guo *et al*, 1987b; Catalano *et al*, 1995). Phi29 DNA-packaging motor and its components have the potential to be used as parts in nanotechnology and as a gene delivery vehicle for cancer treatment (Guo *et al*, 2003; Guo, 2005; Khaled *et al*, 2005) and viral infections (Hoeprich *et al*, 2003). This essential viral replication step has also been investigated in the quest for new antiviral drugs (Zhang *et al*, 1995; Trottier *et al*, 1997; Bogner, 2002). Driving phi29's DNA-packaging motor involves RNA molecules, called pRNA (packaging RNA) (Guo *et al*, 1987a). The crystal structure of the phi29 connector has been reported (Simpson *et al*, 2000; Guasch *et al*, 2002). Direct force measurements of the phi29 motor constructed *in vitro* (Guo *et al*, 1986) have shown that the packaging motor of phi29 is among the most powerful biomotors constructed to date, producing forces up to 57 pN under an external load (Smith *et al*, 2001). Its DNA-packaging rate is estimated to be 2 bp per hydrolyzed ATP (Guo *et al*, 1987b). A major goal in investigation of the phi29 motor is to understand the mechanical and physical behavior of the motor complex and individual motor components. It has been proposed that the mismatch and relative motion between the five-fold procapsid vertexes (Bazinet and King, 1985) and the six-fold connector (a 12-subunit complex) produced a force to drive a rotation motor to stuff DNA (Hendrix, 1978; Chen and Guo, 1997). To make two rings move relatively, at least one additional component is needed to provide a propelling force. There were discrepancies regarding the stoichiometry and the foothold of pRNA as well as which component is stationary and which is moving. One model suggested that pRNA is the moving component and six copies of pRNA bind to the connector and work sequentially (Chen and Guo, 1997). Another model proposed that a pentameric pRNA ring binds to the vertex of the pentameric capsid structure (Simpson *et al*, 2000). Recently, it was found that the foothold for pRNA is not the capsid protein, and that pRNA binds to the N-termini of connector (Xiao *et al*, 2005; Sun *et al*, 2006) that was confirmed to have 12 copies of gp10 (Jimenez *et al*, 1986; Guasch *et al*, 2002). It has also been revealed that pRNA contains two functional domains (Reid *et al*, 1994; Zhang *et al*, 1994), one is the central region of pRNA that binds to the connector and the other locates at the 5′/3′ paired ends that bind to the DNA-packaging enzyme gp16 (Lee and Guo, 2006). Currently, it is still under fervent debate whether the pRNA ring contains six (Chen and Guo, 1997; Guo *et al*, 1998; Zhang *et al*, 1998; Chen *et al*, 2000; Ibarra *et al*, 2000; Fang *et al*, 2005; Robinson *et al*, 2006) or five copies of pRNA (Simpson *et al*, 2000; Morais *et al*, 2001, 2005).

The size of most biomacromolecules, including the phi29 motor, is of nanometer scale, which is too small to be detected and resolved by conventional optical microscopy. The development of optical devices and mechanical probes

*Corresponding author. Purdue Cancer Center, Hansen Life Science Research Building, Purdue University, West Lafayette, IN 47907, USA. Tel.: +1 765 494 7561; Fax: +1 765 496 1795;
E-mail: guop@purdue.edu
[3]These authors contributed equally and share the first authorship

Received: 18 August 2006; accepted: 23 November 2006

that are sensitive enough to measure single molecules has brought about a new era in biomechanical research (Svoboda and Block, 1994; Weiss, 1999; Dohoney and Gelles, 2001; Purcell *et al*, 2005).

Single-molecule detection allows one to understand the structure–function relation for individual biomolecules, as opposed to the ensemble average that is obtained by measurements involving a large population of homogenous molecules that are motionless or require synchronous motion (Vale *et al*, 1996; Ishijima *et al*, 1998; Ha, 2001; Rueda *et al*, 2004). Single-molecule approaches allow for direct observation of physical behavior and provide answers to many questions, such as: how is chemical energy converted into physical motion (Adachi *et al*, 2000; Hirono-Hara *et al*, 2001; Yasuda *et al*, 2001); how is force generated (Svoboda and Block, 1994); how is molecule structure involved in chemical reactions (Zhuang *et al*, 2000; Ha *et al*, 2002); how does the motion start and continue without interruption; how do different motor parts respond to applied force (Chemla *et al*, 2005); and how do conformational changes relate to the production of force (Chemla *et al*, 2005; Jankowsky, 2005; Myong *et al*, 2005; Rondelez *et al*, 2005; Seidel *et al*, 2005). Some of these questions have already been addressed by single-molecule approaches, specifically for RNA ribozyme (Zhuang *et al*, 2000), helicase (Ha *et al*, 2002), RNA polymerase (Wang *et al*, 1998), and other molecular motors such as myosin (Finer *et al*, 1994), kinesin (Svoboda and Block, 1994; Hess *et al*, 2002), and F1-ATPase (Adachi *et al*, 2000). Discovering the answers to these questions will make it possible to elucidate the properties of biomotors and other biological machines, and will also help in the design of novel nanodevices as well as the imitation of natural ones (Soong *et al*, 2000; Tomishige *et al*, 2002; Bringmann *et al*, 2004; Fletcher *et al*, 2005; Pomerantz *et al*, 2005). Here, we report the application of single-molecule approaches to directly observe the translocation of phi29 DNA, and to determine the stoichiometry of one of the vital motor components, pRNA.

Results and discussion

Design and assembly of customized single-molecule dual-viewing total internal reflection fluorescence imaging system with a top prism

The phi29 DNA-packaging motor is in a few tens of nanometer scale, which is beyond the resolution of conventional optical microscopy. We designed and assembled a custom-built imaging system (Figure 1) to detect a single pRNA molecule that was labeled with a single fluorescent dye and to determine the stoichiometry of pRNA in the phi29 DNA-packaging motor. This system includes a customized laser combiner; an optical fiber to deliver multiple laser beams; a dual-view imager to separate the emitted fluorescence signals of different wavelengths to facilitate the signal analysis; a cooling system of $-70^{\circ}C$ to reduce background noise; a detector with electron multiplier; and a prism located at the top of the perfusion chamber instead of at the bottom, thus reducing the possible influence of both the background noise in solution and the leakage to the objective lens of the reflected laser light. Owing to these modifications, this system produces strong and stable signals with extremely low background noise for the detection of single fluorophores on pRNA.

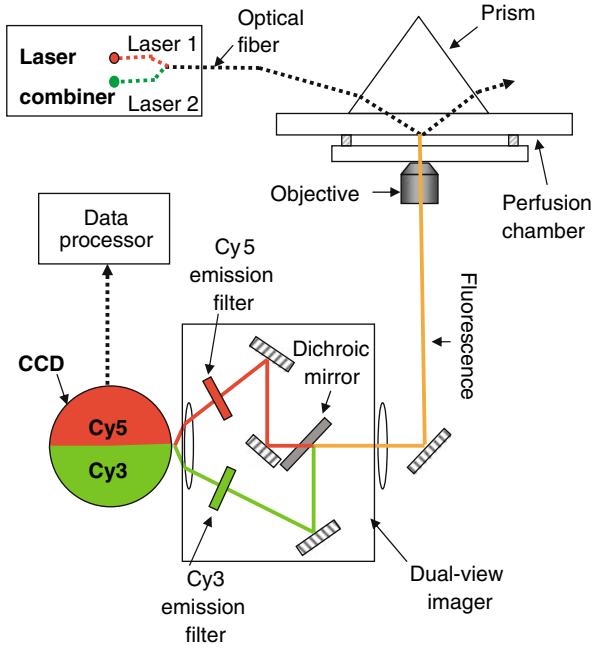

Figure 1 Setup of the SMDV-TIRF.

Counting of pRNA on procapsid/pRNA complex using single-molecule dual-viewing total internal reflection fluorescence imaging system with a top prism

To determine the stoichiometry of pRNA for each DNA-packaging motor, it is critical to know (1) how many copies of pRNA bind to the procapsid before DNA packaging and (2) how many copies of pRNA are working on the motor during the DNA translocation process.

Before assessing the copy number of pRNA on the active motor (see section Counting of pRNA on the motor that was actively translocating DNA), the copy number of pRNA on the procapsid before initiation of DNA packaging was investigated. Each wild-type pRNA molecule was labeled with one Cy3 fluorophore and purified before attachment to the procapsid of the phi29 DNA-packaging motor (Figure 2A). The portion of fluorescent pRNA with energizable Cy3 fluorophore that can produce quantized photobleaching steps was about $70 \pm 3\%$, as determined by spectrometer and empirical titration (see section *In vitro* synthesis of fluorescent pRNA and titration of pRNA-labeling efficiency). Purified Cy3-pRNA was biologically active in procapsid binding and DNA packaging, as evidenced by *in vitro* phi29 virion assembly (Lee and Guo, 1995). Purified procapsid/pRNA complexes containing Cy3-pRNA were imaged by single-molecule dual-viewing total internal reflection fluorescence imaging system with a top prism (SMDV-TIRF), after immobilization in a perfusion chamber through anti-procapsid IgG (Figure 2B). Photobleaching events were recorded. The Cy3-containing procapsid/pRNA complexes appeared as distinct bright spots with an even and dark background under the microscope. The change of fluorescence intensity for each spot with time revealed a distribution in 1–6 steps of photobleaching (Figure 3Aa–f). With each spot representing one procapsid/pRNA complex, the height of each step was almost equal within

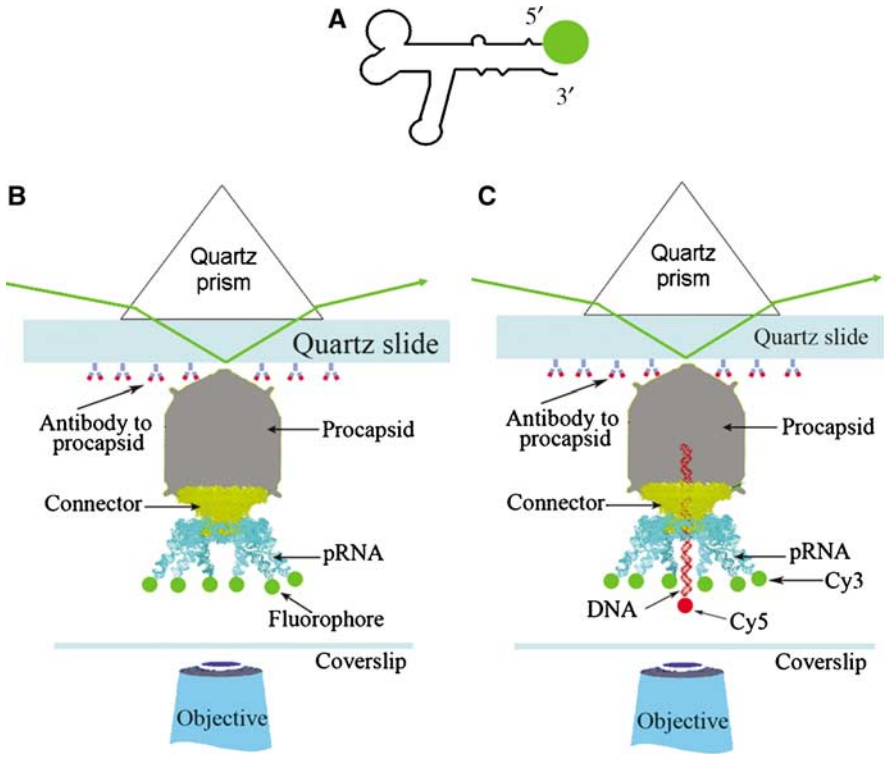

Figure 2 Experiment design for single-molecule imaging. (**A**) pRNA with a fluorescent label at its 5′ end. (**B**) Experimental design for quantized photobleaching of fluorescent pRNA in procapsid/pRNA complexes. (**C**) Experimental design for quantized photobleaching of dual-labeled DNA-packaging intermediates containing Cy3-pRNA and Cy5-DNA.

each motor, indicating that each step came from the photobleaching of a single Cy3 molecule.

A total of 1736 spots were analyzed and grouped by the number of steps. In the resulting histogram showing the photobleaching steps (Figure 3B), the number above each column indicates the total counts of events for each group with the specific number of steps. The comparisons of empirical data with parameters predicted from the four models are presented in Figure 3C (see section Statistical analysis). There were some rare events showing more than six steps, which could be due to the nonspecific aggregation. This low count is insignificant and negligible compared to the counts at steps equal to or less than six.

When the procapsid/pRNA complexes were constructed with RNA dimers (Guo *et al*, 1998; Chen *et al*, 2000), which were composed of one Cy3-pRNA I and one Cy5-pRNA II (Figure 4A), dual-color fluorescence images were obtained as shown in Figure 4B. Most of the fluorescent spots showed yellow color, resulting from the overlay from red (Cy5 signal) and green (Cy3 signal). The colors are pseudo-color representations of the fluorescence. This revealed that most of the procapsids contained both Cy3-pRNA I and Cy5-pRNA II, as the pRNA was expected to bind to procapsids in a manner similar to its dimeric form (Chen *et al*, 2000). Fluorescence intensity change with time for each yellow spot was plotted to show photobleaching steps for Cy3- and Cy5-pRNA separately. Figure 4D shows a typical three steps of photobleaching in both Cy3 signal (green) and Cy5 signal (red) for the yellow spots analyzed. The count for each specific number of photobleaching steps for Cy3-pRNA I is summarized and compared with theoretical prediction by the histograms in Figure 4C.

Statistical analysis

Current debate on the mechanism of pRNA function focuses on whether the pRNA ring is a hexamer or pentamer. To address this, different models were proposed for the distribution in photobleaching steps. These models were evaluated from the *z*-score (relative distribution of the measurements) and *P*-value (observed significance level) in model fittings for the distribution of photobleaching steps (see section Statistical analysis of models for pRNA stoichiometry). The following four models from A to D were tested:

Algorithm for modeling and computation:

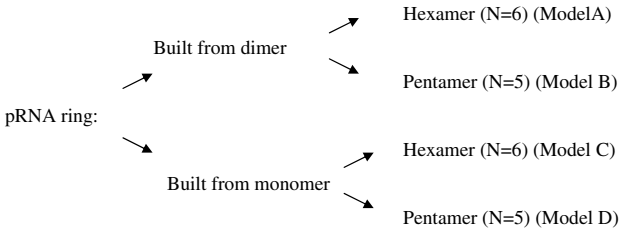

The 70% Cy3 labeling efficiency of this batch of pRNA was used for model predictions. In Figure 3C, the empirical distribution for procapsid/Cy3-pRNA complexes was compared with statistical models A–D. The *z*-score and *P*-value (Table I) indicate the fitting quality; the lower the *z*-score or the higher the *P*-value, the better the fitting. The data revealed that only the model for a hexamer assembled from dimers was reasonable, with a relatively small *z*-score (2.8) and a relatively large *P*-value (0.2%). The other three models (see section Statistical analysis of models for pRNA

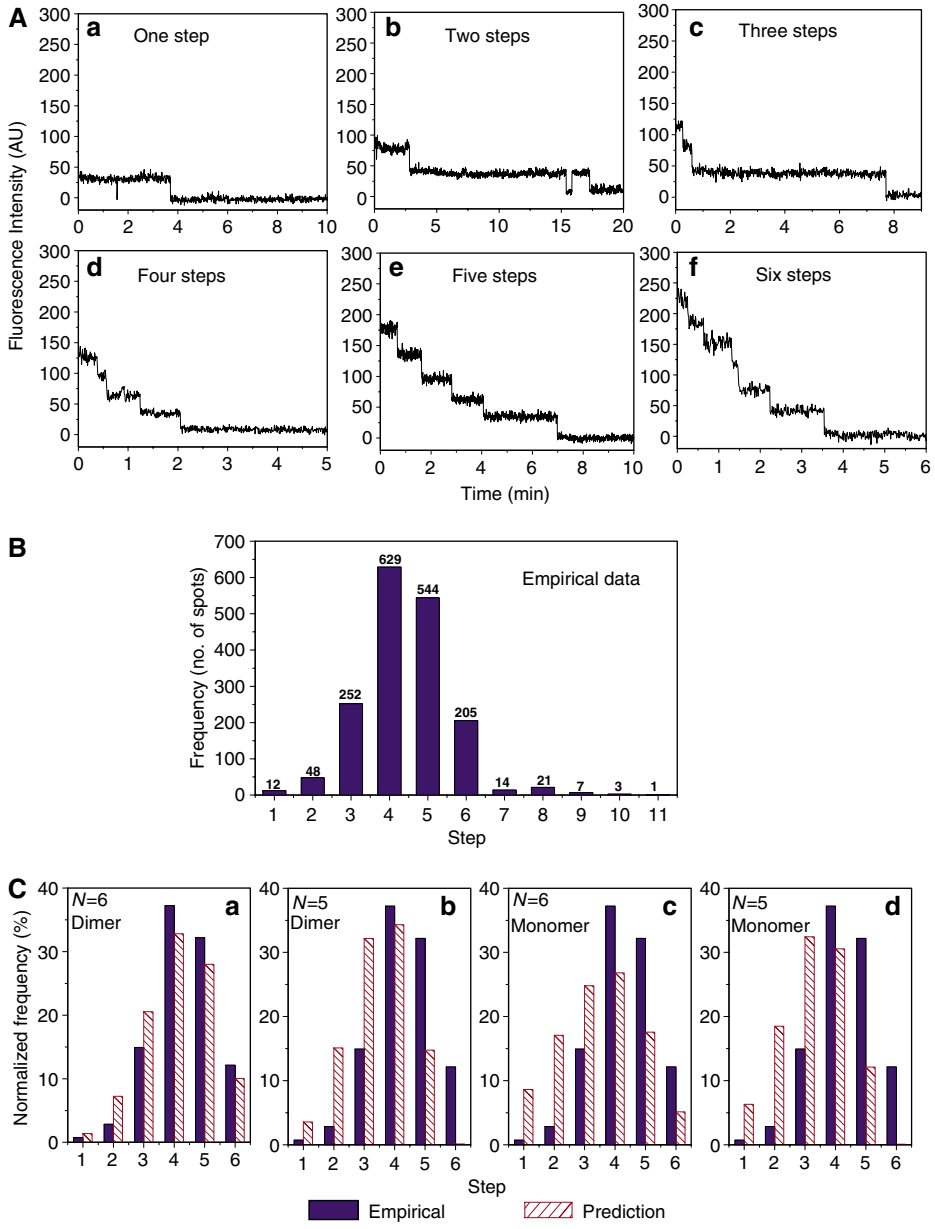

Figure 3 Photobleaching analysis of procapsid/Cy3-pRNA complex. (**A**) Plots of fluorescence intensity versus time for Cy3-pRNA in procapsid/pRNA complexes that showed one, two, three, four, five, and six steps in photobleaching. The intensity was plotted in arbitrary units. (**B**) Empirical histogram of procapsid/Cy3-pRNA complex showing the distribution frequency of 1736 spots grouped by steps of quantized photobleaching. (**C**) Statistic model fitting of empirical histogram of photobleaching steps. The empirical data were compared with model predictions. (a) Model A; (b) Model B; (c) Model C; (d) Model D.

stochiometry) were excluded as the corresponding *z*-scores are large and *P*-values are extremely small. Statistical analysis led to the conclusion that the pRNA ring is a hexamer that is assembled from dimers.

Owing to the partial degradation and incomplete labeling of RNA, the number of motors that appear to have five photobleaching steps far exceeds those that show six steps, as shown in Figure 3B. Such an inclination toward the side of the smaller copy number might lead to the conclusion of a lesser stoichiometry by the other imaging methods, and could lead to the misconception that the pRNA copy number in the active phi29 motor is five instead of six.

Counting of pRNA on the motor that was actively translocating DNA

One argument for the discrepancy of the pRNA hexamer and pentamer is that pRNA might assemble onto the procapsid as a hexamer before DNA packaging, but one pRNA of the hexameric ring might be shifted out of the ring or eliminated (Simpson *et al*, 2000). Model B in section Statistical analysis represents the hypothesis that three of the dimers were assembled into procapsids as hexamer and one of the pRNA diffused away. Even though this model was excluded by statistics (see section Statistical analysis), it is still important to count the copy number of pRNA on the motor that is actively packaging DNA. To ensure that the DNA packaging

for procapsid was initiated but not completed, and the motor was in its active intermediate state of DNA translocation, the distal left *Eco*RI fragment of phi29 genome was used as a packaging substrate. This fragment was only half the length of the phi29 genomic DNA and contained all packaging signals, including the terminal protein gp3 (Grimes and Anderson, 1989; Blanco *et al*, 1994), whereas its right end was ligated with a short single-stranded DNA oligo conjugated with a Cy5 (or biotin, see the next section). In this case, the DNA packaging was halted by the single-stranded region (Moll and Guo, 2005) or by non-hydrolyzable γ-S-ATP (Shu and Guo, 2003) (see section Direct observation of DNA translocation). The DNA-packaging intermediates with partially packaged and partially protruding single-stranded DNA were isolated by sucrose gradient sedimentation (Shu and Guo, 2003) (Figure 5A) to separate them from the free pRNA, free DNA, and the procapsid/pRNA complexes that did not contain DNA. In addition to Cy5 labeling in DNA, each pRNA in these intermediates was labeled with Cy3 (Figure 2C).

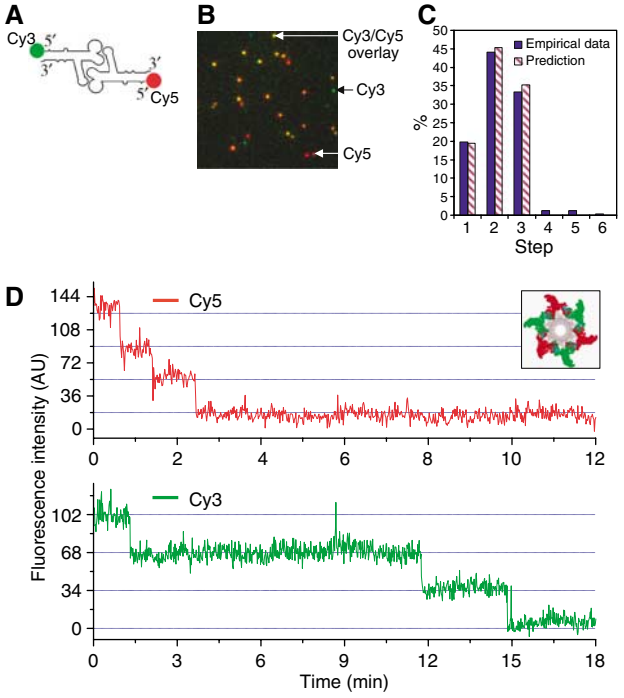

Figure 4 Dual-view imaging of procapsids containing both Cy3-pRNA I and Cy5-pRNA II. (**A**) pRNA dimer constructed with Cy3-pRNA I and Cy5-pRNA II. (**B**) Typical fluorescence image of procapsids bound with dual-labeled pRNA dimers. The image is an overlay from the fluorescence signals in both Cy3 and Cy5 channels, presented in pseudo-colors. Signals in the Cy3 channel were assigned green and those in the Cy5 channel were assigned red. Yellow color resulted from the overlay of red and green. Green color spots are procapsid/pRNA complexes containing Cy3 only; red color spots are the complexes containing Cy5 only. The yellow color spots are the combination of green and red, representing coexistence of Cy3-pRNA I and Cy5-pRNA II on one procapsid. (**C**) Comparison of empirical distribution with theoretical prediction in photobleaching steps of Cy3-pRNA I in procapsids bound with dual-labeled dimers. Prediction was based on a 70% labeling efficiency of Cy3-pRNA. (**D**) Fluorescence intensity versus time to show photobleaching steps of procapsids reconstituted with the dimer, elucidated in the inset showing procapsids with a pRNA hexamer composed of three Cy3-pRNA I and three Cy5-pRNA II.

The purified intermediates were confirmed by colocalization of Cy5-DNA and Cy3-pRNA with SMDV-TIRF using dual-color images (Figure 5Bb, inset). The green spots represent procapsids/Cy3-pRNA that did not contain Cy5-conjugated DNA; the red spots represent procapsids containing Cy5-DNA with unlabeled pRNA; the yellow spots represent procapsids containing both Cy3-pRNA and Cy5-DNA, which are the DNA-packaging intermediates (Figure 5Bb, inset). The distribution of the yellow spots (intermediates) and red spots (Cy5-DNA) among the gradient fractions was plotted (Figure 5A). Confirmation that these intermediates contained DNA was supported by the finding that the peak representing Cy5-DNA in the intermediates overlaps with the peak representing the dual-labeled intermediates in the gradient (Figure 5Ac).

The copy number of pRNA in the DNA-packaging intermediates was determined by photobleaching assay. In this case, only the dual-color spots (yellow spots), signifying the presence of both pRNA and DNA, were analyzed. The histogram of photobleaching steps of Cy3-pRNA reveals that the distribution matched the profile predicted by the pRNA hexamer model ($N=6$), but did not match the profile predicted with the pRNA pentamer model ($N=5$) (Figure 5B).

Direct observation of DNA translocation

To ensure that the functional intermediates were isolated, non-hydrolyzable γ-S-ATP was used to stall the motor (Shu and Guo, 2003). After attaching to a slide coated with anti-procapsid IgG, the motor function was restored by addition of ATP, and observed at real time by fluorescence microscopy. In this case, a biotin moiety was attached to the distal right end of the phi29 genomic DNA and linked to a fluorescent streptavidin-coated microsphere, which was observed by fluorescence microscopy (Figure 6A) and its motion was

Table I Parameters in statistical analysis

	Z	*P*	*a*	*b*	*c*	*d*	*e*	*f*
Dimer								
A. $N=6$	2.8	2.2×10^{-3}	0	0	1	n/a	n/a	n/a
B. $N=5$	144	8.8×10^{-4545}	0	0	1	n/a	n/a	n/a
Monomer								
C. $N=6$	13	3.2×10^{-38}	0.015	0.045	0.058	0.070	0.161	0.651
D. $N=5$	160	1.6×10^{-5567}	0.010	0.016	0.048	0.113	0.813	n/a

Summarized results for model fitting, showing the *z* score, *P*-value and predicted fraction of procapsids that have (*a*) 1, (*b*) 2 or (*c*) 3 pRNA dimers bound in dimer models; predicted fraction of procapsids that have (*a*) 1, (*b*) 2, (*c*) 3, (*d*) 4, (*e*) 5 or (*f*) 6 pRNA bound in monomer models.
n/a: not applicable.

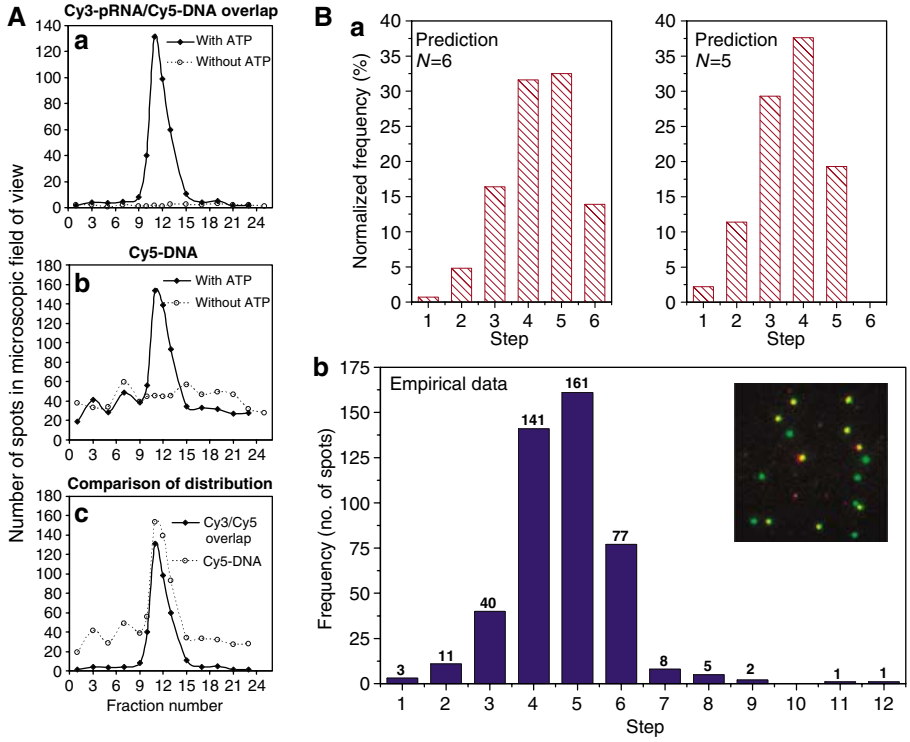

Figure 5 Determination of pRNA stoichiometry during DNA translocation within DNA-packaging intermediates containing both Cy3-pRNA and Cy5-DNA. (**A**) Distribution of the DNA-packaging intermediates in sucrose gradient. (a) Distribution of yellow spots resulted from overlay of Cy3 and Cy5. (b) Distribution of red spot intermediates with single Cy5 label on DNA. (c) Comparison of the distribution of red spots (Cy5-DNA) and yellow spots (intermediates with pRNA and DNA). (**B**) Comparison of the empirical group distribution (b) with the predicted distribution of hexamer ($N=6$) or pentamer ($N=5$) (a). Inset: a typical pseudo-color image of the dual-labeled intermediates. Red represents Cy5, green represents Cy3, and yellow represents overlay from Cy3 and Cy5.

analyzed in x, y and z dimensions. Without the addition of ATP, microspheres exhibited a mainly linear and unchanging Brownian motion. In contrast, when the restart solution with ATP was added, DNA migration caused the attached microsphere to show a gradual reduction in swing range (Figure 6Ca and b). Finally, the motion stopped owing to the physical restriction of DNA being completely packaged and appeared under the CCD camera as a zero distance change from the reference origin. This provides conclusive evidence that the intermediates demonstrate a true DNA-packaging event and further indicates that the motors within the DNA-containing procapsid were functional in DNA translocation.

Direct observation of pRNA–ferritin complexes on procapsid by EM

Ferritin is a spherical multisubunit protein about 11 nm in diameter. It has an iron core, which makes it electron-dense and a useful label for transmission electron microscopy. For stoichiometric investigation, the ferritin was conjugated with streptavidin to facilitate binding to the biotin at the 3′ end of pRNA. Procapsids with six ferritin molecules were observed (Figure 7), providing further evidence that the stoichiometry of pRNA was six.

pRNA trimer had the highest activity and was the most sensitive to heat dissociation, followed by the dimer and then the monomer

Previous studies have revealed that both the engineered pRNA dimer and trimer are active in phi29 DNA packaging (Guo *et al*, 1998; Zhang *et al*, 1998), strongly suggesting that the stoichiometry of pRNA on the procapsid is an even number, or the common multiple of 2 and 3, thus automatically excluding 5 as a possible value. It could be argued that the dimer or trimer serves only as one active building unit, allowing for 10 (five dimers) or 15 (five trimers) to bind the procapsid (if it were a pentamer). It is necessary to confirm that: (1) the purified pRNA dimer (assembly pathway model 1; Figure 8Aa) or trimer (assembly pathway model 2; Figure 8Ab) alone can serve as true intermediates to assemble virion, (2) each pRNA in the dimer or trimer plays its role and (3) the ring is not composed of 10 or 15 (multiples of 5) pRNAs when the pRNA dimer or trimer is used. The purified pRNA dimer and trimer were compared with the pRNA monomer (present in solution as a mixture of equal molar concentrations of monomeric building blocks) for their sensitivities to heat dissociation. If the trimer and dimer were not true intermediates in motor assembly but served as only one unit, the activity of pRNA would be increased after dissociation into monomers as the molar concentration would increase two- or three-fold, respectively, after heat dissociation, which does not interfere with pRNA monomer activity. Figure 8B shows that the trimer is the most sensitive to heat dissociation, whereas monomers are not significantly affected by heat dissociation and dimers fall in between. These results further indicate that both dimers and trimers are stable and can serve as true intermediates in viral DNA packaging. The dimeric and trimeric pRNA served as two- or three-unit entities, respectively, in DNA packaging. Given that 6 is the least common multiple of 2 and 3 (representing dimer and trimer), this further confirms that the stoichiometry of pRNA in the phi29 motor is six.

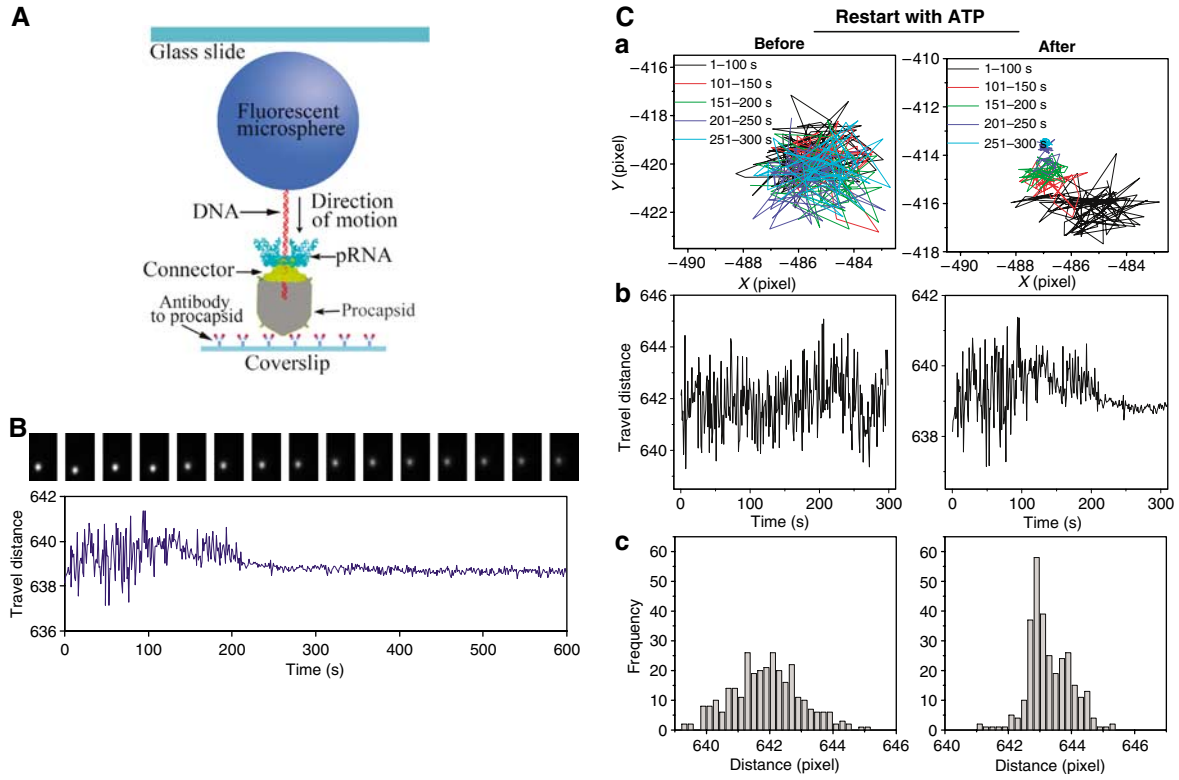

Figure 6 Direct observation of phi29 DNA translocation (packaging). (**A**) Experimental design for direct observation of phi29 DNA translocation. In the packaging intermediate, the DNA is labeled with a fluorescent microsphere (graph not drawn to scale). (**B**) Sequential images of a fluorescent microsphere attached to DNA (top), and plot of swinging range (distance) versus time (bottom) during DNA packaging. (**C**) Comparison of the motion track of a microsphere attached to an intermediate before and after the addition of ATP. (a) Trajectories of the fluorescent microsphere. Different colors represent a different time range during the translocation. (b) Change of microsphere's travel distance (swinging range) during the course of DNA translocation. (c) Histogram of frequency for the travel distance of the microsphere.

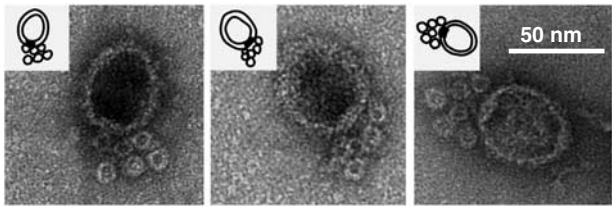

Figure 7 Negatively stained EM images of procapsids containing pRNA conjugated with ferritin.

Materials and methods

Setup of SMDV-TIRF

The microscope setup is depicted in Figure 1. An Olympus IX71 inverted microscope was used with a ×60 objective (PlanApo, NA = 1.4, oil immersion) to collect fluorescence signal. Signal was recorded with an Andor iXon 887 V EMCCD camera (Andor Technology). For dual-color fluorescence imaging, both 638 nm (laser 1) and 532 nm (laser 2) beams were delivered by the laser combiner for simultaneous excitation. Fluorescence signals were collected through the objective and split to Cy3 and Cy5 channels through Dual-View™ imager (Optical Insights, LLC). After the blueprint was designed, the mounting parts for the assembly of the prism on the top of the stage were instrumentally fabricated by the machine shop in the College of Engineering at Purdue.

In vitro synthesis of fluorescent pRNA and titration of pRNA-labeling efficiency

Methods for 5′-end labeling of pRNA with a single chemical group have been reported (Garver and Guo, 2000; Huang, 2003; Guo *et al*, 2006). Such labeling (Figure 2A) was achieved with *in vitro* transcription by T7 RNA polymerase using dsDNA templates containing the T7 class II promoter (Ø2.5) in the presence of 2 mM Cy3- or Cy5-AMP labeled with a single fluorophore. Single AMP can be used by the polymerase only for initiation and not chain extension, which requires a triphosphate. This method ensures that each pRNA contains only one Cy3 or Cy5 at its 5′ end. Electrophoresis under denatured condition was used to separate and purify the labeled pRNA from the unlabeled pRNA. After cutting the band out of the gel and elution, homogeneous pRNA with one Cy3 (or Cy5) was obtained, as determined by gel electrophoresis of the purified products. RNA concentration was determined by a UV/Vis spectrophotometer (Beckman DU530) at an OD 260, whereas Cy3 concentration was obtained by measuring the absorbance at 550 nm ($\varepsilon_{550\,nm} = 150\,000$). Labeling efficiency was calculated as the molar concentration of Cy3 divided by the molar concentration of pRNA. This efficiency was also confirmed by binomial distribution in photobleaching steps of Cy3-pRNA dimers incubated with the DNA-packaging components in the absence of purified procapsid. The portion of energizable Cy3 fluorophore that can produce quantized photobleaching steps was determined specifically for each batch of pRNA and was found to be 70 ± 3%.

Photobleaching assay of procapsid/fluorescent pRNA complexes

Procapsid/fluorescent pRNA complexes were isolated from free pRNA by 5–20% sucrose gradient sedimentation with Beckman SW55 rotor for 35 min at 35 000 r.p.m. The purified procapsid/fluorescent pRNA complexes were immobilized on the surface of a perfusion chamber by anti-procapsid IgG (Proteintech Group Inc.) (Figure 2B). Excess procapsid/pRNA complexes were removed by washing. The focused beam was about 150 × 50 μm. The concentration of the samples was adjusted to show discrete fluorescing spots in the images. Laser power was adjusted to be 8 mW to photobleach the fluorophore at a reasonable speed so that the steps of photobleaching were easily distinguished. Sequential images were taken with an exposure time of 200–400 ms at 1 s intervals. The recorded movies were analyzed by the computer program of

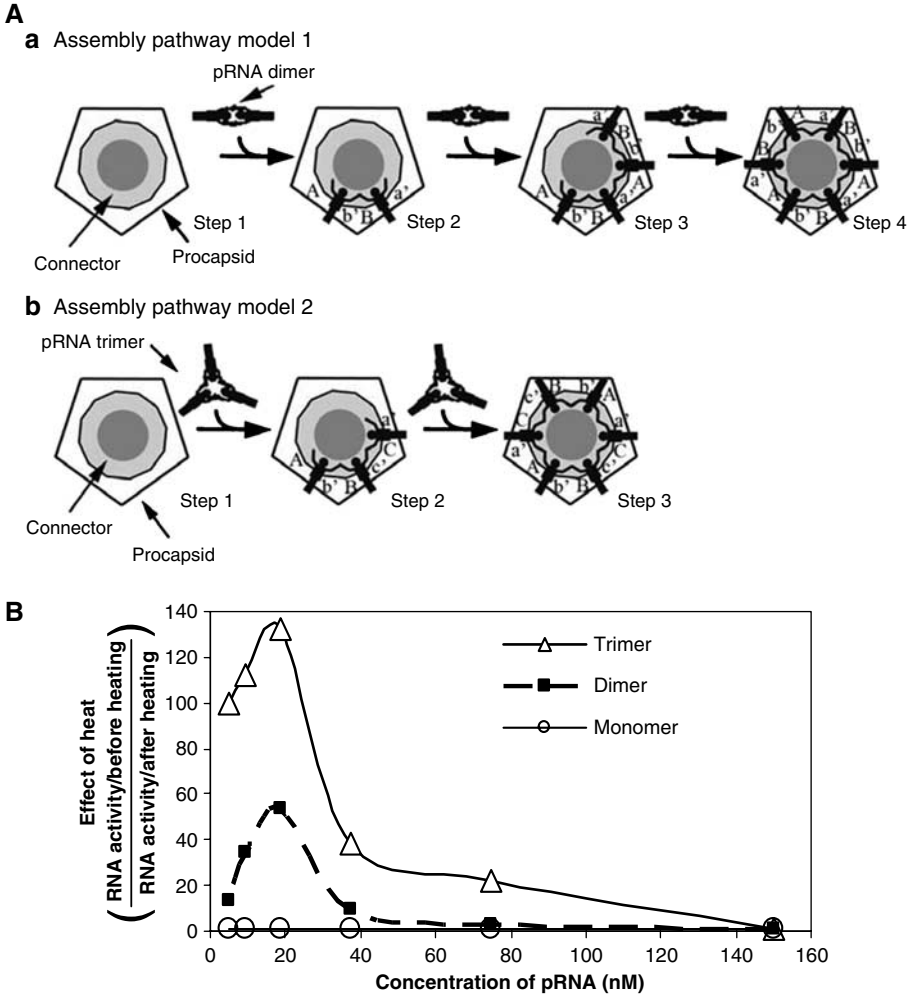

Figure 8 (**A**) Models for assembly pathways of pRNA hexameric ring. (**B**) Effect of heat dissociation on the activity (PFU/ml) of pRNA monomer, dimmer, and trimer. The *y*-axis is the factor (effect of heat) resulting from the activity (PFU/ml) of non-heated pRNA divided by the activity of heated pRNA, that is, the quotient of pRNA activity before heating (x) divided by the activity after heating (y). 'Background effect' indicates that when the pRNA is at a very low concentration where the activity is extremely low, the background noise, m, could cover up the activity and the difference before and after heating could not be revealed. When x and y are small, $(x+m)/(y+m)$ will approach 1. 'Effect by K_d of dimer and trimer' indicates that higher pRNA concentrations result in a smaller effect of heating, as dimer and trimer could reform again quickly after denaturation at high concentrations.

Kinetic Imaging (Andor Technology) to give the plots of fluorescence intensity versus time for each spot.

Fluorescent labeling of the EcoRI fragment of phi29 DNA

The left *Eco*RI fragment of phi29 DNA-gp3 was purified and then ligated with a synthetic DNA fragment containing the *Eco*RI sticky end with a Cy5 tag attached to the extended single-stranded DNA. For labeling with fluorescent beads, biotinylated DNA-gp3 was prepared as described above, with oligonucleotides containing a biotin moiety instead of Cy5. All labeled DNAs were purified from gel to homogeneity.

Photobleaching assay of dual-labeled DNA-packaging intermediates

Methods for the isolation of DNA-packaging intermediates have been described (Shu and Guo, 2003). Photobleaching assay on purified active intermediates was carried out with a similar approach as for procapsid/pRNA complexes. The distribution of the intermediates in sucrose gradient was determined by counting the red (representing Cy5-DNA) and yellow (representing motors containing both Cy3-pRNA and Cy5-DNA) spots within the microscopic field of view for samples from each gradient fraction.

Direct observation of DNA translocation

The stalled packaging intermediates containing biotinylated DNA were prepared by using non-hydrolyzable γ-S-ATP (Shu and Guo, 2003). The intermediates were then immobilized to perfusion chambers built from glass slides and coverslips (Figure 6A). The 0.53 μm fluorescent streptavidin microspheres (Bangs Laboratories Inc.) were bound to the protruding, biotinylated DNA end of the intermediates. After restarting the packaging reaction by adding gp16 and ATP (Shu and Guo, 2003), an individual DNA-packaging event was observed. Epi-illumination was used. Sequential images with 8-bit digital resolution were recorded at 1 frame per second for 600 s. The pixel resolution of the images was 0.26 μm/pixel.

Computer analysis of DNA translocation

To confirm DNA migration and to distinguish the DNA-packaging event from nonspecific Brownian motion, the images recorded were analyzed with Andor Tracker software (Andor Technology). For the first step of the analysis, the movement trajectory of the microsphere was traced on a computer and pixilated in the x and y directions, during the course of packaging. The second step of the analysis was to plot the travel distance (pixels) to a reference point in the image versus time (s).

Direct observation of ferritin–pRNA complex by EM

The pRNA-ferritin conjugates were prepared by hybridizing an oligo, which was linked to one ferritin particle to its 5′ end, with the 26-nucleotides that extended from the 3′ end of the pRNA. By changing the molar ratio of the nucleotide and the particle, the conjugate, composed of only one ferritin per pRNA, was isolated by a single band excited from agarose gel, and attached to procapsid.

The pRNA–ferrin complexes not bound to the procapsid were removed by ultracentrifugation before negative-stained EM.

Biochemical assay of specific activity for monomer, dimer, and trimer

pRNA was heated to 90°C and purified from a denaturing gel before being assembled into a dimer or trimer to ensure that all RNA molecules in the population did not contain single-stranded nicks. The dimer and trimer were separated from monomer by purification with 8% native polyacrylamide gel in TBM buffer (89 mM Tris, 200 mM boric acid, 5 mM $MgCl_2$, pH 7.6). Before the activity assay, the purity and 'intactness' (without nicks) of each sample was re-examined after heating at 90°C by denaturing gel. To compare the motor assembly and DNA-packaging activities, the monomer, dimer, and trimer were subjected to serial dilution in TMS. Each dilution was divided into two parallel groups. Group one was heated to 90°C to dissociate the dimer (or trimer) into monomer and the other remained as an unheated dimer or trimer. The activity of pRNA for each group was titrated with the *in vitro* phi29 assembly system (Lee and Guo, 1995).

Statistical analysis of models for pRNA stoichiometry

The statistical analysis included three steps.

Step 1, modeling. Statistical models were setup in a way such that each model is totally specified except for a few unknown parameters.

Step 2, fitting models. The observed data from the experiment were used to fit each model and obtain an estimate for each parameter.

Step 3, evaluating models. All four models were evaluated using the estimated parameters. The model that best fits the empirical data was accepted, with all others rejected. It was then concluded whether the pRNA ring is more likely to be a hexamer or a pentamer.

For the first step, four models were utilized as shown in Figure 3C. Model A and C stand for hexamer models, whereas model B and D stand for pentamer models. Model A and B also stand for a model with pRNA ring assembled from the dimers. Similarly, model C and D also stand for another model with the pRNA ring assembled from monomers.

For the second step, it was considered that only the fluorescent RNAs labeled with the dye Cy3 were observable and could be counted. Empirical data provide the observed fraction of procapsids containing exactly i molecules of Cy3, where $i=1, 2,\ldots, 6$, out of the total number of observed procapsids that contain at least one Cy3 molecule (Figure 3B). By assuming a few unknown parameters and using the model specified above, mathematical formulas were developed to predict the fraction with i fluorescent pRNA, where $1\leqslant i\leqslant 6$. Comparing the observed fraction and the predicted fraction, statistical analysis was carried out to determine which set of parameters is the best-fit for the empirical data.

To describe the mathematical formulas in detail, we focused on model A ($N=6$, assembled from dimer). Similar approaches were carried out for the other three models. For model A, $N=6$, and each procapsid could contain 0, 1, 2, or 3 dimers. First, as empty procapsids are never observable, it was proposed that among non-empty procapsids, the fractions of those that contain 1, 2, and 3 dimers are a, b, and c; clearly, $a+b+c=1$ or $c=1-a-b$. It was found previously that the binding of pRNA to procapsid is cooperative with a Hill constant of 2.5 (Chen *et al*, 2000); therefore, $a\leqslant b\leqslant c$. Second, suppose that there is a total of k RNA in the procapsid. As the labeling efficiency is 70%, the number of fluorescent dye Cy3 is distributed as binomial (k, 0.7), for example, the chance of having exactly i Cy3 equals $\binom{k}{i}\,0.7^i\times 0.3^{k-i}$.

Next, for $0\leqslant i\leqslant 6$, denote f_i as the fraction of procapsids containing exactly i molecules of Cy3. The observation in the above paragraph enables the calculation of f_i explicitly. As an example, suppose $i=1$: then, 1 Cy3 on a procapsid can contain 1, 2, or 3 dimers, making the total fraction of procapsids having 1 Cy3 equal to

$$f_1(a,b)=a\binom{2}{1}0.7\times 0.3+b\binom{4}{1}0.7\times 0.33+(1-a-b)\binom{6}{1}0.7\times 0.3^5$$

Last, note that a procapsid containing 0 molecules of Cy3 (although it can have several pRNA) can never be observed, allowing the predicted fractions to be written as

$$\frac{f_i}{1-f_0}=\frac{f_i(a,b)}{1-f_0(a,b)},\quad 1\leqslant i\leqslant 6$$

The criterion of mean-squared error (MSE) was used to locate which pairs of (a,b) is the best-fit with the empirical data. The MSE is defined as the average squares of discrepancy between the observable fraction and the predicted fraction, which is a function of (a,b):

$$\mathrm{MSE}(a,b)=\frac{1}{6}\sum_{i=1}^{6}\left(y_i-\frac{f_i(a,b)}{1-f_0(a,b)}\right)^2$$

where y_i can be obtained from Figure 3B. A Matlab code was then programmed to search which pairs of (a,b) gave the best-fit or the smallest MSE value.

The next step was to use the fitted values to evaluate the model. As the goal is to determine whether the pRNA ring is a hexamer or a pentamer, the focus is on the fraction of six molecules of Cy3. Suppose the pair of $(a=\hat{a}, b=\hat{b})$ gave the best-fit, by inserting $(\hat{a},\hat{b})$ back into the model, the z-score could be calculated as

$$z=\sqrt{T}\,\frac{y_6-\dfrac{f_6(\hat{a},\hat{b})}{1-f_0}}{\sqrt{\dfrac{f_6(\hat{a},\hat{b})}{1-f_0(\hat{a},\hat{b})}\left(1-\dfrac{f_6(\hat{a},\hat{b})}{1-f_0(\hat{a},\hat{b})}\right)}}$$

where T is the total number of observed procapsids containing at least one molecule of Cy3. The rationale behind the z-score is that, when the model is accurate, z-score is approximately distributed as standard Gaussian (i.e. $N(0,1)$) and should be relatively small. An unusually large z-score implies that the model is not accurate. Equivalently, the P-values were determined by $P=\mathrm{P}\{|N(0,1)|\geqslant|z|\}$. An unusually small P-value implies that the model is not accurate.

Acknowledgements

We thank Wulf-Dieter Moll, David Rueda, Nils Walter, Chris Meiners, Meredith Lambert, Peter Stockley, Taekjip Ha, Toshio Yanagida, Faqing Huang, Masasuke Yoshida, Kazuhiko Kinosita Jr and Eckhard Jankowsky for their technical assistance and valuable comments. The research on determination of pRNA schoichiometry by biological and chemical approaches was supported by NIH grant R01-GM59944, and the project on motor conjugation was supported by R01-EB03730 from the National Institute of Biomedical Imaging and Bioengineering.

References

Adachi K, Yasuda R, Noji H, Itoh H, Harada Y, Yoshida M, Kinosita Jr K (2000) Stepping rotation of F1-ATPase visualized through angle-resolved single-fluorophore imaging. *Proc Natl Acad Sci USA* **97:** 7243–7247

Bazinet C, King J (1985) The DNA translocation vertex of dsDNA bacteriophages. *Annu Rev Microbiol* **39:** 109–129

Blanco L, Lazaro JM, de Vega M, Bonnin A, Salas M (1994) Terminal protein-primed DNA amplification. *Proc Natl Acad Sci USA* **91:** 12198–12202

Bogner E (2002) Human cytomegalovirus terminase as a target for antiviral chemotherapy. *Rev Med Virol* **12:** 115–127

Bringmann H, Skiniotis G, Spilker A, Kandels-Lewis S, Vernos I, Surrey T (2004) A kinesin-like motor inhibits microtubule dynamic instability. *Science* **303:** 1519–1522

Catalano CE, Cue D, Feiss M (1995) Virus DNA packaging: the strategy used by phage lambda. *Mol Microbiol* **16:** 1075–1086

Chemla YR, Aathavan K, Michaelis J, Grimes S, Jardine PJ, Anderson DL, Bustamante C (2005) Mechanism of force

generation of a viral DNA packaging motor. *Cell* **122:** 683–692
Chen C, Guo P (1997) Sequential action of six virus-encoded DNA-packaging RNAs during phage phi29 genomic DNA translocation. *J Virol* **71:** 3864–3871
Chen C, Sheng S, Shao Z, Guo P (2000) A dimer as a building block in assembling RNA. A hexamer that gears bacterial virus phi29 DNA-translocating machinery. *J Biol Chem* **275:** 17510–17516
Cue D, Feiss M (2001) Bacteriophage lambda DNA packaging: DNA site requirements for termination and processivity. *J Mol Biol* **311:** 233–240
Dohoney KM, Gelles J (2001) Chi-sequence recognition and DNA translocation by single RecBCD helicase/nuclease molecules. *Nature* **409:** 370–374
Fang Y, Cai Q, Qin PZ (2005) The procapsid binding domain of phi29 packaging RNA has a modular architecture and requires 2′-hydroxyl groups in packaging RNA interaction. *Biochemistry* **44:** 9348–9358
Finer JT, Simmons RM, Spudich JA (1994) Single myosin molecule mechanics: piconewton forces and nanometre steps. *Nature* **368:** 113–119
Fletcher SP, Dumur F, Pollard MM, Feringa BL (2005) A reversible, unidirectional molecular rotary motor driven by chemical energy. *Science* **310:** 80–82
Garver K, Guo P (2000) Mapping the inter-RNA interaction of phage phi29 by site-specific photoaffinity crosslinking. *J Biol Chem* **275:** 2817–2824
Grimes S, Anderson D (1989) *In vitro* packaging of bacteriophage phi29 DNA restriction fragments and the role of the terminal protein gp3. *J Mol Biol* **209:** 91–100
Guasch A, Pous J, Ibarra B, Gomis-Ruth FX, Valpuesta JM, Sousa N, Carrascosa JL, Coll M (2002) Detailed architecture of a DNA translocating machine: the high-resolution structure of the bacteriophage phi29 connector particle. *J Mol Biol* **315:** 663–676
Guo P (1994) Introduction: principles, perspectives, and potential applications in viral assembly. *Semin Virol (Editor's Introduction)* **5:** 1–3
Guo P (2005) RNA Nanotechnology: engineering, assembly and applications in detection, gene delivery and therapy. *J Nanosci Nanotechnol* **5:** 1964–1982
Guo P, Erickson S, Anderson D (1987a) A small viral RNA is required for *in vitro* packaging of bacteriophage phi29 DNA. *Science* **236:** 690–694
Guo P, Grimes S, Anderson D (1986) A defined system for *in vitro* packaging of DNA-gp3 of the *Bacillus subtilis* bacteriophage phi29. *Proc Natl Acad Sci USA* **83:** 3505–3509
Guo P, Peterson C, Anderson D (1987b) Prohead and DNA-gp3-dependent ATPase activity of the DNA packaging protein gp16 of bacteriophage phi29. *J Mol Biol* **197:** 229–236
Guo P, Zhang C, Chen C, Trottier M, Garver K (1998) Inter-RNA interaction of phage phi29 pRNA to form a hexameric complex for viral DNA transportation. *Mol Cell* **2:** 149–155
Guo S, Huang F, Guo P (2006) Construction of folate-conjugated pRNA of bacteriophage phi29 DNA packaging motor for delivery of chimeric siRNA to nasopharyngeal carcinoma cells. *Gene Therapy* **13:** 814–820
Guo S, Shu D, Simon M, Guo P (2003) Gene cloning, purification and stoichiometry quantification of phi29 anti-receptor gp12 with potential use as special ligand for gene delivery. *Gene* **315:** 145–152
Ha T (2001) Single-molecule fluorescence resonance energy transfer. *Methods* **25:** 78–86
Ha T, Rasnik I, Cheng W, Babcock HP, Gauss GH, Lohman TM, Chu S (2002) Initiation and re-initiation of DNA unwinding by the *Escherichia coli* Rep helicase. *Nature* **419:** 638–641
Hendrix RW (1978) Summetry mismatch and DNA packaging in large bacteriophages. *Proc Natl Acad Sci USA* **75:** 4779–4783
Hess H, Howard J, Vogel V (2002) A piconewton forcemeter assembled from microtubules and kinesins. *Nano Lett* **2:** 1113–1115
Hirono-Hara Y, Noji H, Nishiura M, Muneyuki E, Hara KY, Yasuda R, Kinosita Jr K, Yoshida M (2001) Pause and rotation of F(1)-ATPase during catalysis. *Proc Natl Acad Sci USA* **98:** 13649–13654
Hoeprich S, ZHou Q, Guo S, Qi G, Wang Y, Guo P (2003) Bacterial virus phi29 pRNA as a hammerhead ribozyme escort to destroy hepatitis B virus. *Gene Therapy* **10:** 1258–1267
Huang F (2003) Efficient incorporation of CoA, NAD and FAD into RNA by *in vitro* transcription. *Nucleic Acids Res* **31:** e8
Ibarra B, Caston JR, Llorca O, Valle M, Valpuesta JM, Carrascosa JL (2000) Topology of the components of the DNA packaging machinery in the phage phi29 prohead. *J Mol Biol* **298:** 807–815
Ishijima A, Kojima H, Funatsu T, Tokunaga M, Higuchi H, Tanaka H, Yanagida T (1998) Simultaneous observation of individual ATPase and mechanical events by a single myosin molecule during interaction with actin. *Cell* **92:** 161–171
Jankowsky E (2005) Biophysics: helicase snaps back. *Nature* **437:** 1245
Jimenez J, Santisteban A, Carazo JM, Carrascosa JL (1986) Computer graphic display method for visualizing three-dimensional biological structures. *Science* **232:** 1113–1115
Khaled A, Guo S, Li F, Guo P (2005) Controllable self-assembly of nanoparticles for specific delivery of multiple therapeutic molecules to cancer cells using RNA nanotechnology. *Nano Lett* **5:** 1797–1808
Lee CS, Guo P (1995) *In vitro* assembly of infectious virions of ds-DNA phage phi29 from cloned gene products and synthetic nucleic acids. *J Virol* **69:** 5018–5023
Lee TJ, Guo P (2006) Interaction of gp16 with pRNA and DNA for genome packaging by the motor of bacterial virus phi29. *J Mol Biol* **356:** 589–599
Lin H, Black LW (1998) DNA requirements *in vivo* for phage T4 packaging. *Virology* **242:** 118–127
Moll D, Guo P (2005) Translocation of nicked but not gapped DNA by the packaging motor of bacteriophage phi29. *J Mol Biol* **351:** 100–107
Morais MC, Choi KH, Koti JS, Chipman PR, Anderson DL, Rossmann MG (2005) Conservation of the capsid structure in tailed dsDNA bacteriophages: the pseudoatomic structure of phi29. *Mol Cell* **18:** 149–159
Morais MC, Tao Y, Olsen NH, Grimes S, Jardine PJ, Anderson D, Baker TS, Rossmann MG (2001) Cryoelectron-microscopy image reconstruction of symmetry mismatches in bacteriophage phi29. *J Struct Biol* **135:** 38–46
Myong S, Rasnik I, Joo C, Lohman TM, Ha T (2005) Repetitive shuttling of a motor protein on DNA. *Nature* **437:** 1321–1325
Pomerantz RT, Ramjit R, Gueroui Z, Place C, Anikin M, Leuba S, Zlatanova J, McAllister WT (2005) A tightly regulated molecular motor based upon T7 RNA polymerase. *Nano Lett* **5:** 1698–1703
Purcell T, Sweeney HL, Spudich JA (2005) A force-dependent state controls the coordination of processive myosin V. *Proc Natl Acad Sci USA* **102:** 13873–13878
Reid RJD, Bodley JW, Anderson D (1994) Characterization of the prohead–pRNA interaction of bacteriophage phi29. *J Biol Chem* **269:** 5157–5162
Robinson MA, Wood JP, Capaldi SA, Baron AJ, Gell C, Smith DA, Stonehouse NJ (2006) Affinity of molecular interactions in the bacteriophage phi29 DNA packaging motor. *Nucleic Acids Res* **34:** 2698–2709
Rondelez Y, Tresset G, Nakashima T, Kato-Yamada Y, Fujita H, Takeuchi S, Noji H (2005) Highly coupled ATP synthesis by F1-ATPase single molecules. *Nature* **433:** 773–777
Rueda D, Bokinsky G, Rhodes MM, Rust MJ, Zhuang X, Walter NG (2004) Single-molecule enzymology of RNA: essential functional groups impact catalysis from a distance. *Proc Natl Acad Sci USA* **101:** 10066–10071
Seidel R, Bloom JG, van NJ, Dutta CF, Dekker NH, Firman K, Szczelkun MD, Dekker C (2005) Dynamics of initiation, termination and reinitiation of DNA translocation by the motor protein *Eco*R124I. *EMBO J* **24:** 4188–4197
Shu D, Guo P (2003) Only one pRNA hexamer but multiple copies of the DNA-packaging protein gp16 are needed for the motor to package bacterial virus phi29 genomic DNA. *Virology* **309:** 108–113
Simpson AA, Tao Y, Leiman PG, Badasso MO, He Y, Jardine PJ, Olson NH, Morais MC, Grimes S, Anderson DL, Baker TS, Rossmann MG (2000) Structure of the bacteriophage phi29 DNA packaging motor. *Nature* **408:** 745–750
Smith DE, Tans SJ, Smith SB, Grimes S, Anderson DL, Bustamante C (2001) The bacteriophage phi29 portal motor can package DNA against a large internal force. *Nature* **413:** 748–752
Soong RK, Bachand GD, Neves HP, Olkhovets AG, Craighead HG, Montemagno CD (2000) Powering an inorganic nanodevice with a biomolecular motor. *Science* **290:** 1555–1558
Sun J, Cai Y, Moll WD, Guo P (2006) Controlling bacteriophage phi29 DNA-packaging motor by addition or discharge of a peptide

at N-terminus of connector protein that interacts with pRNA. *Nucleic Acids Res* **34:** 5482–5490

Svoboda K, Block SM (1994) Force and velocity measured for single kinesin molecules. *Cell* **77:** 773–784

Tomishige M, Klopfenstein DR, Vale RD (2002) Conversion of Unc104/KIF1A kinesin into a processive motor after dimerization. *Science* **297:** 2263–2267

Trottier M, Garver K, Zhang C, Guo P (1997) DNA-packaging pRNA as target for complete inhibition of viral assembly *in vitro* and *in vivo*. *Nucleic Acids Symp Ser* **36:** 187–189

Vale RD, Funatsu T, Pierce DW, Romberg L, Harada Y, Yanagida T (1996) Direct observation of single kinesin molecules moving along microtubules. *Nature* **380:** 451–453

Wang MD, Schnitzer MJ, Yin H, Landick R, Gelles J, Block SM (1998) Force and velocity measured for single molecules of RNA polymerase. *Science* **282:** 902–907

Weiss S (1999) Fluorescence spectroscopy of single biomolecules. *Science* **283:** 1676–1683

Xiao F, Moll D, Guo S, Guo P (2005) Binding of pRNA to the N-terminal 14 amino acids of connector proteinof bacterial phage phi29. *Nucleic Acids Res* **33:** 2640–2649

Yasuda R, Noji H, Yoshida M, Kinosita Jr K, Itoh H (2001) Resolution of distinct rotational substeps by submillisecond kinetic analysis of F1-ATPase. *Nature* **410:** 898–904

Zhang CL, Garver K, Guo P (1995) Inhibition of phage phi29 assembly by antisense oligonucleotides targeting viral pRNA essential for DNA packaging. *Virology* **211:** 568–576

Zhang CL, Lee C-S, Guo P (1994) The proximate 5′ and 3′ ends of the 120-base viral RNA (pRNA) are crucial for the packaging of bacteriophage phi29 DNA. *Virology* **201:** 77–85

Zhang F, Lemieux S, Wu X, St.-Arnaud S, McMurray CT, Major F, Anderson D (1998) Function of hexameric RNA in packaging of bacteriophage phi29 DNA *in vitro*. *Mol Cell* **2:** 141–147

Zhuang X, Bartley LE, Babcock HP, Russell R, Ha T, Herschlag D, Chu S (2000) A single-molecule study of RNA catalysis and folding. *Science* **288:** 2048–2051